Supporting Information

Linker micro-regulation of a Hofmann-based metal–organic framework for efficient propylene/propane separation

Puxu Liu,[a] Kaiming Chen,[a] Yang Chen,[a] Xiaoqing Wang,[a] Jiangfeng Yang,[a] Libo Li,[a,b,*] and Jinping Li,[a,b]

[a] *College of Chemistry and Chemical Engineering, Shanxi Key Laboratory of Gas Energy Efficient and Clean Utilization, Taiyuan University of Technology, Taiyuan, 030024, Shanxi, P. R. China.*

[b] *Key Laboratory of Coal Science and Technology, Ministry of Education and Shanxi Province, Taiyuan University of Technology, Taiyuan 030024, Shanxi, P. R. China*

**Corresponding authors E-mail: lilibo908@hotmail.com*

To *Inorganic Chemistry Frontiers*

Table of contents

1. The structure of CoNi-piz along different directions 3

2. Characterization 4

2.1. Powder X-ray diffraction (PXRD) 4

2.2. N_2 sorption isotherm at 77 K 5

2.3. Scanning Electron Microscopy (SEM) 6

2.4. EDS mapping of the synthesized CoNi-pyz 7

2.5. EDS mapping of the synthesized CoNi-piz 8

3. Adsorption isotherms for C_3H_8 and C_3H_6 of CoNi-pyz and CoNi-piz 9

4. Fitting curves for C_3H_6 and C_3H_8 adsorption isotherms 10

4.1. Fitting curves for CoNi-pyz based on different model 10

4.2. Fitting curves for CoNi-piz based on different model 11

5. IAST selectivity 12

6. Isosteric heat of adsorption 13

6.1. Virial fitting curves and the calculated adsorption heat for CoNi-pyz 13

6.2. Virial fitting curves and the calculated adsorption heat for CoNi-piz 14

7. Dynamic breakthrough experiment 15

8. Dynamic adsorption and desorption for C_3H_6 and C_3H_8 16

9. Dynamic breakthrough experiment under water vapor. 17

10. Supplementary tables 18

10.1. Dynamic capture capacity for C_3H_6 and C_3H_8 at mixed gas condition 19

1. The structure of CoNi-piz along different directions

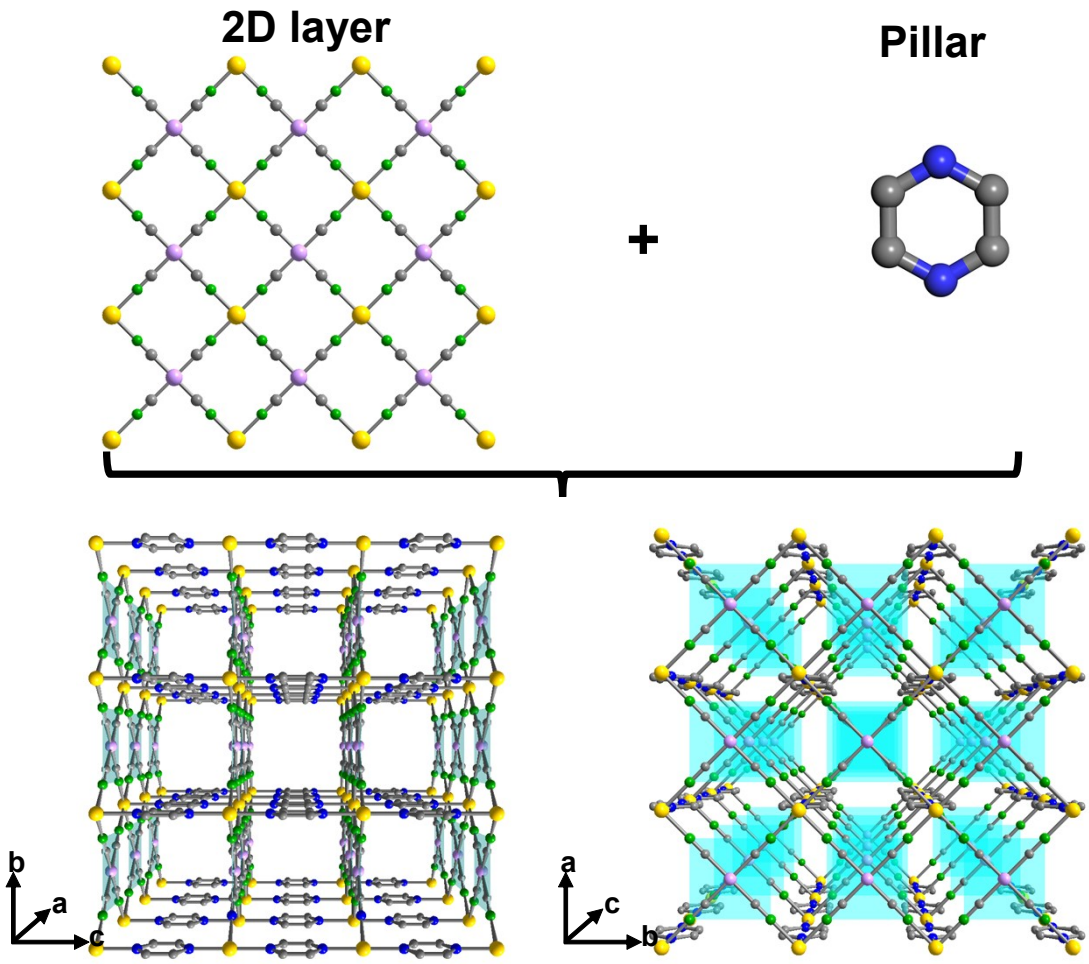

Figure S1. The illustration of assemble process for CoNi-piz, and the structure of resulted scaffold along different directions. (Ni, purple; Co, yellow; N, green and blue; C, gray)

2. Characterization

2.1. Powder X-ray diffraction (PXRD)

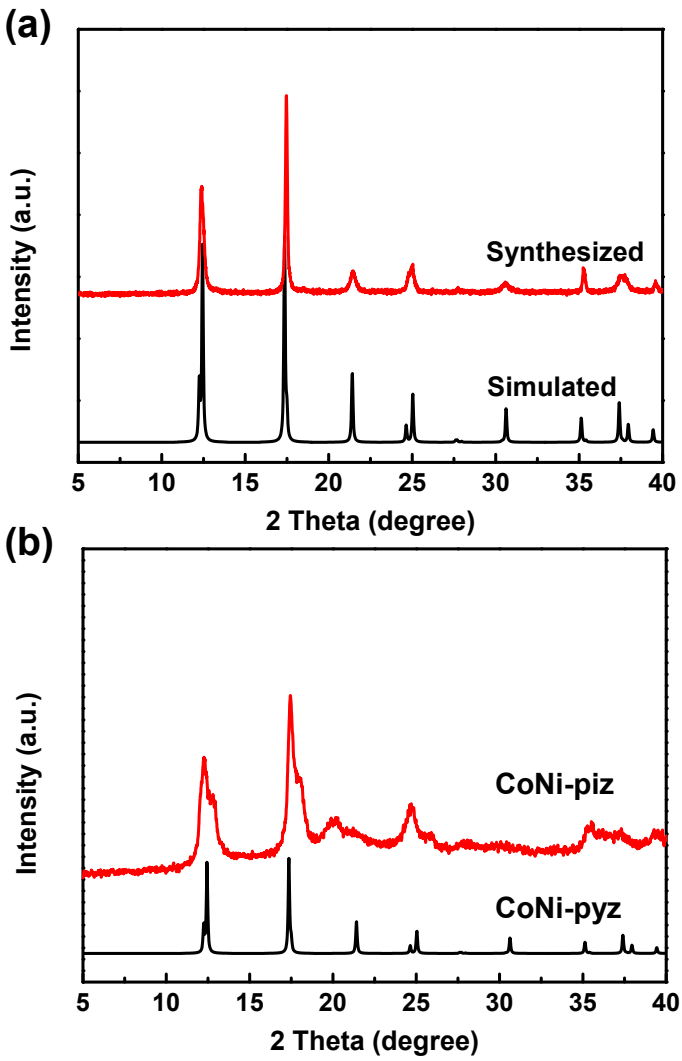

Figure S2. Powder X-ray diffraction (PXRD) patterns of the synthesized CoNi-pyz (a) and CoNi-piz (b).

2.2. N_2 sorption isotherm at 77 K

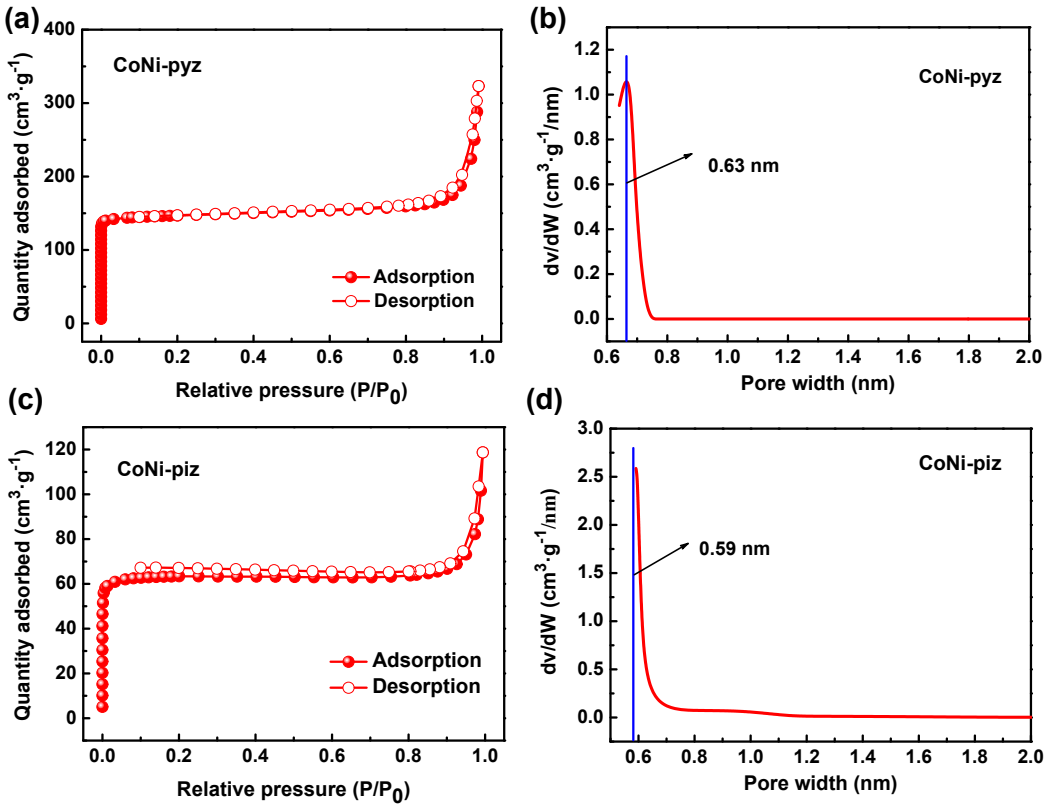

Figure S3. N_2 sorption isotherms and corresponding pore size distribution for the synthesized CoNi-pyz (a-b) and CoNi-piz (c-d).

2.3. Scanning Electron Microscopy (SEM)

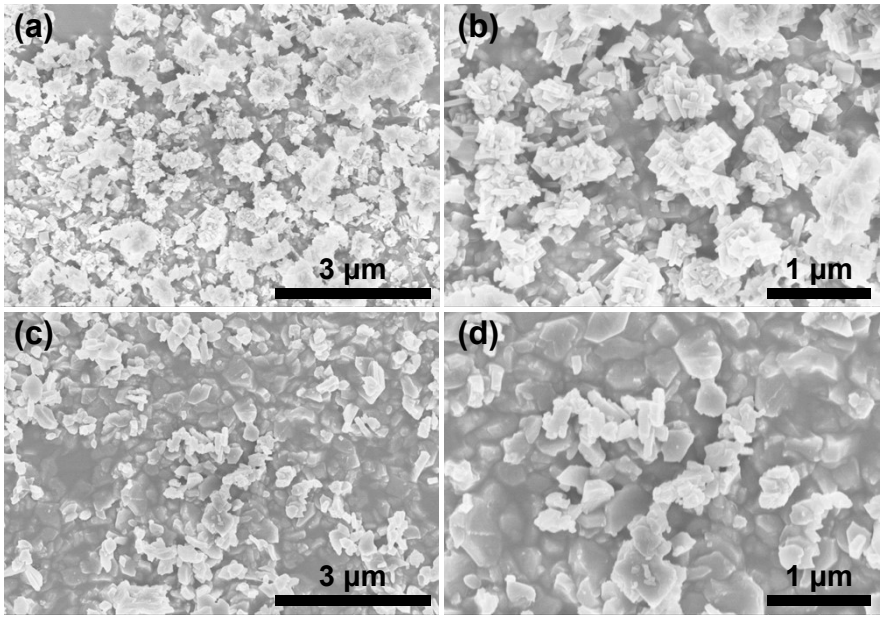

Figure S4. SEM images of the synthesized CoNi-pyz (a-b) and CoNi-piz (c-d) with different magnification.

2.4. EDS mapping of the synthesized CoNi-pyz

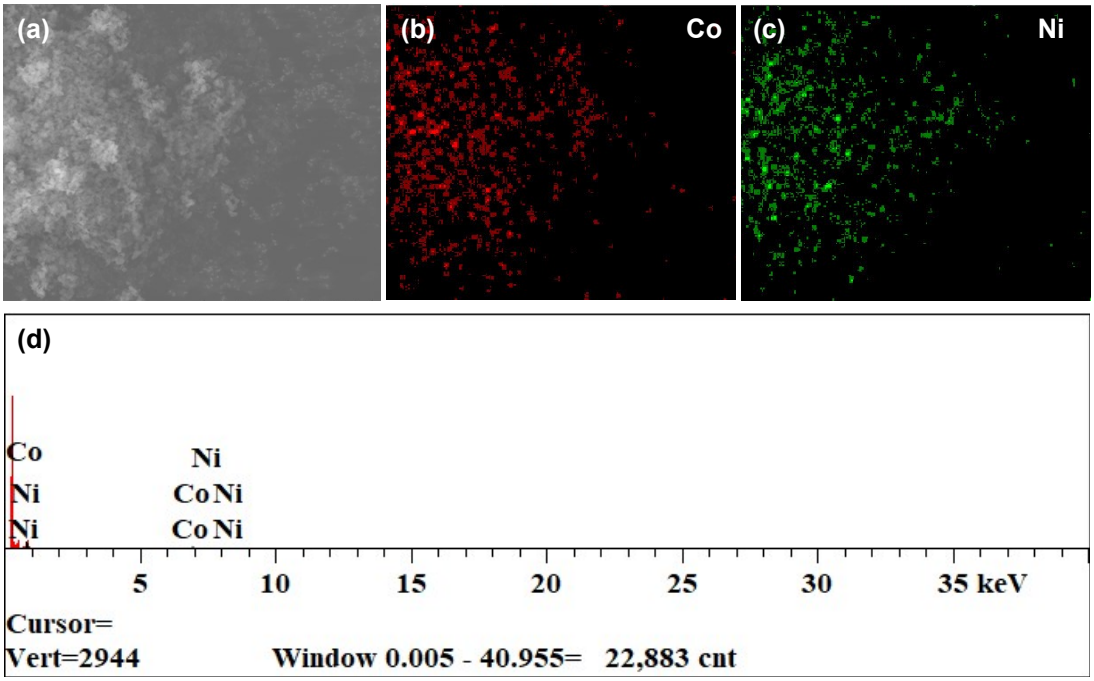

Elt.	Line	Intensity (c/s)	Conc.	Units	
Co	Ka	13.58	48.303	wt.%	
Ni	Ka	11.59	51.697	wt.%	
			100.000	Wt.%	Total

Figure S5. The EDS mapping of the synthesized CoNi-pyz, which showing the almost same content of Cobalt and Nickel of the structure.

2.5. EDS mapping of the synthesized CoNi-piz

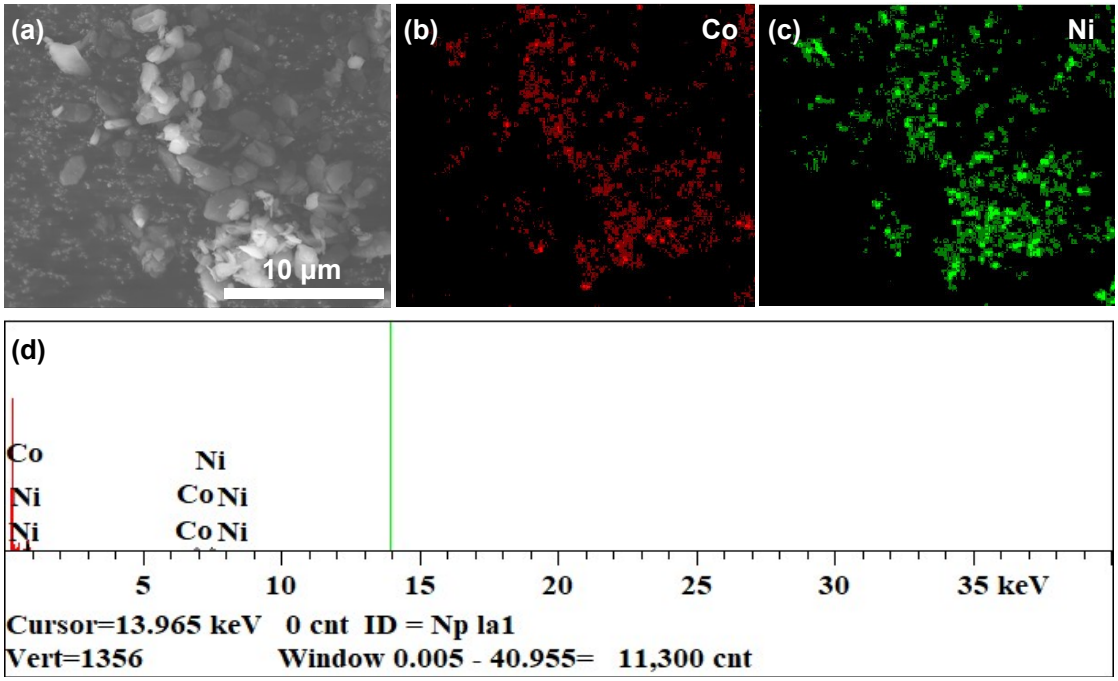

Elt.	Line	Intensity (c/s)	Conc.	Units	
Co	Ka	11.91	49.388	wt.%	
Ni	Ka	9.73	50.612	wt.%	
			100.000	Wt.%	Total

Figure S6. The EDS mapping of the synthesized CoNi-piz, which showing the almost same content of Cobalt and Nickel of the structure.

3. Adsorption isotherms for C_3H_8 and C_3H_6 of CoNi-pyz and CoNi-piz

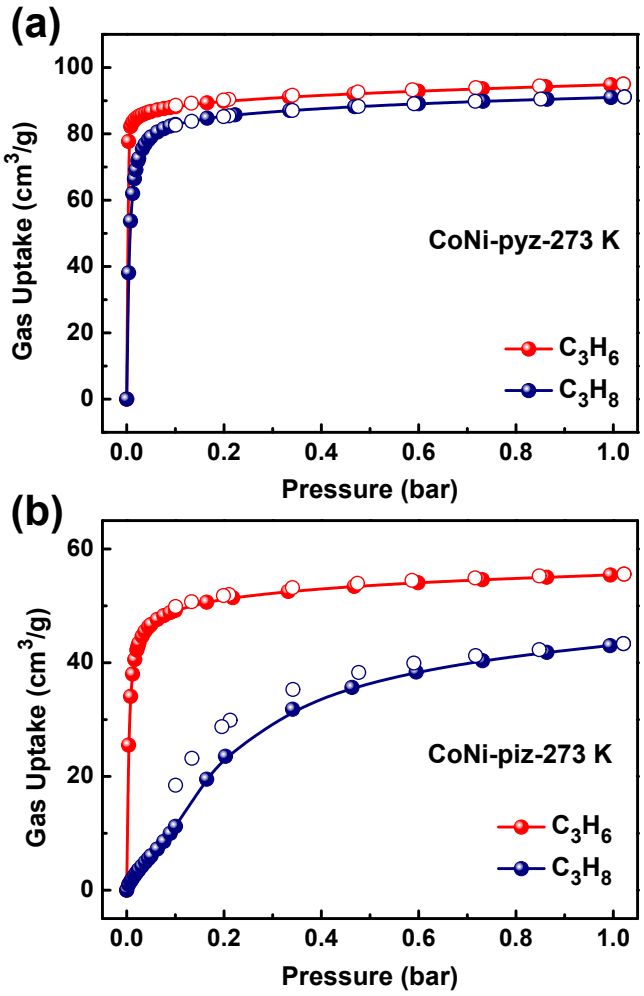

Figure S7. Adsorption (solid) and desorption (open) isotherms for C_3H_8 (blue) and C_3H_6 (red) of CoNi-pyz (a) and CoNi-piz (b) at 273 K up to 1 bar.

4. Fitting curves for C_3H_6 and C_3H_8 adsorption isotherms

4.1. Fitting curves for CoNi-pyz based on different model

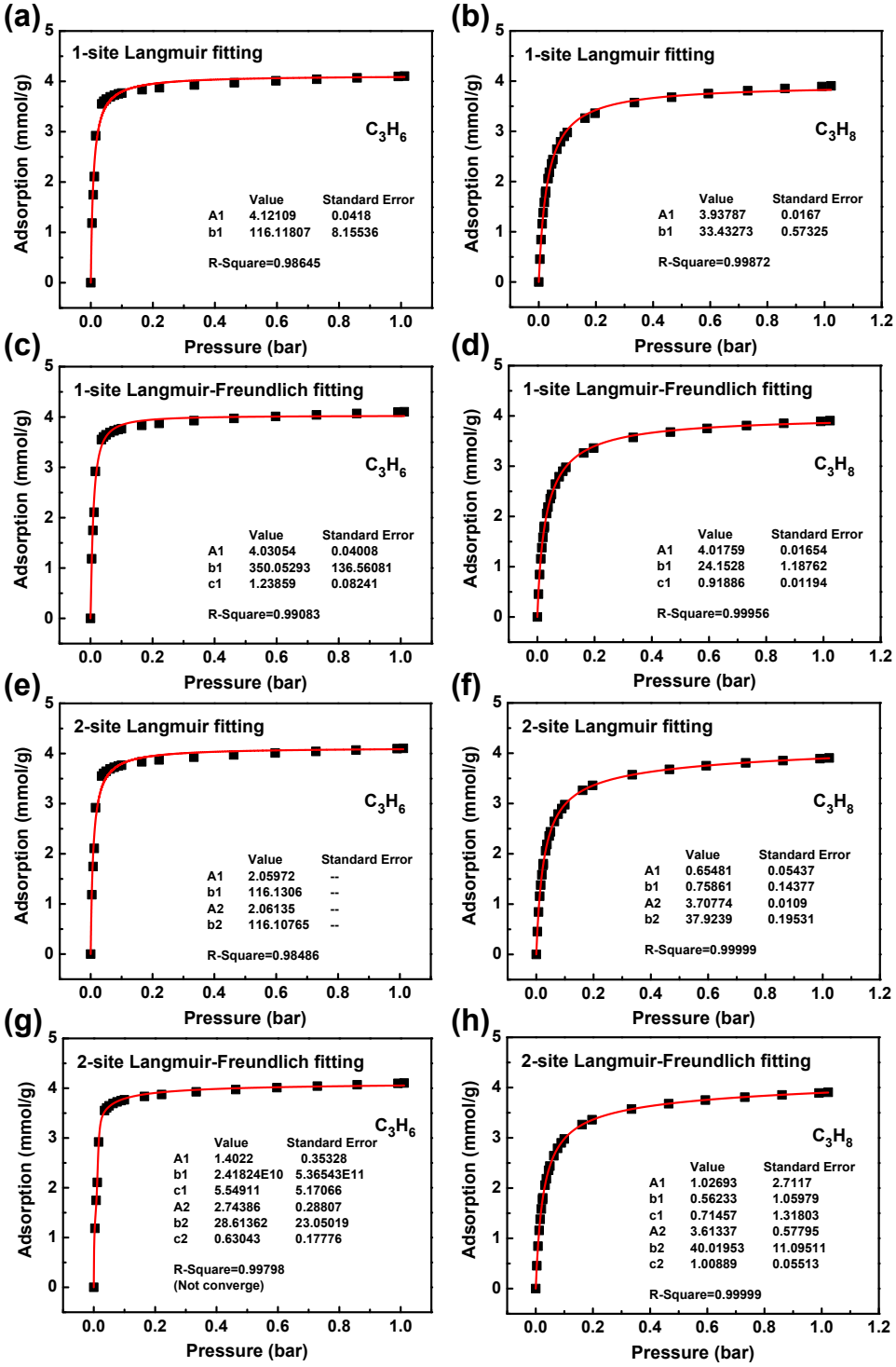

Figure S8. Fitting curves for C_3H_6 and C_3H_8 adsorption isotherms at 298 K and 1 bar based on different adsorption model, and fitting parameters of 1-site Langmuir-Freundlich model were used to calculate IAST selectivity for CoNi-pyz.

4.2. Fitting curves for CoNi-piz based on different model

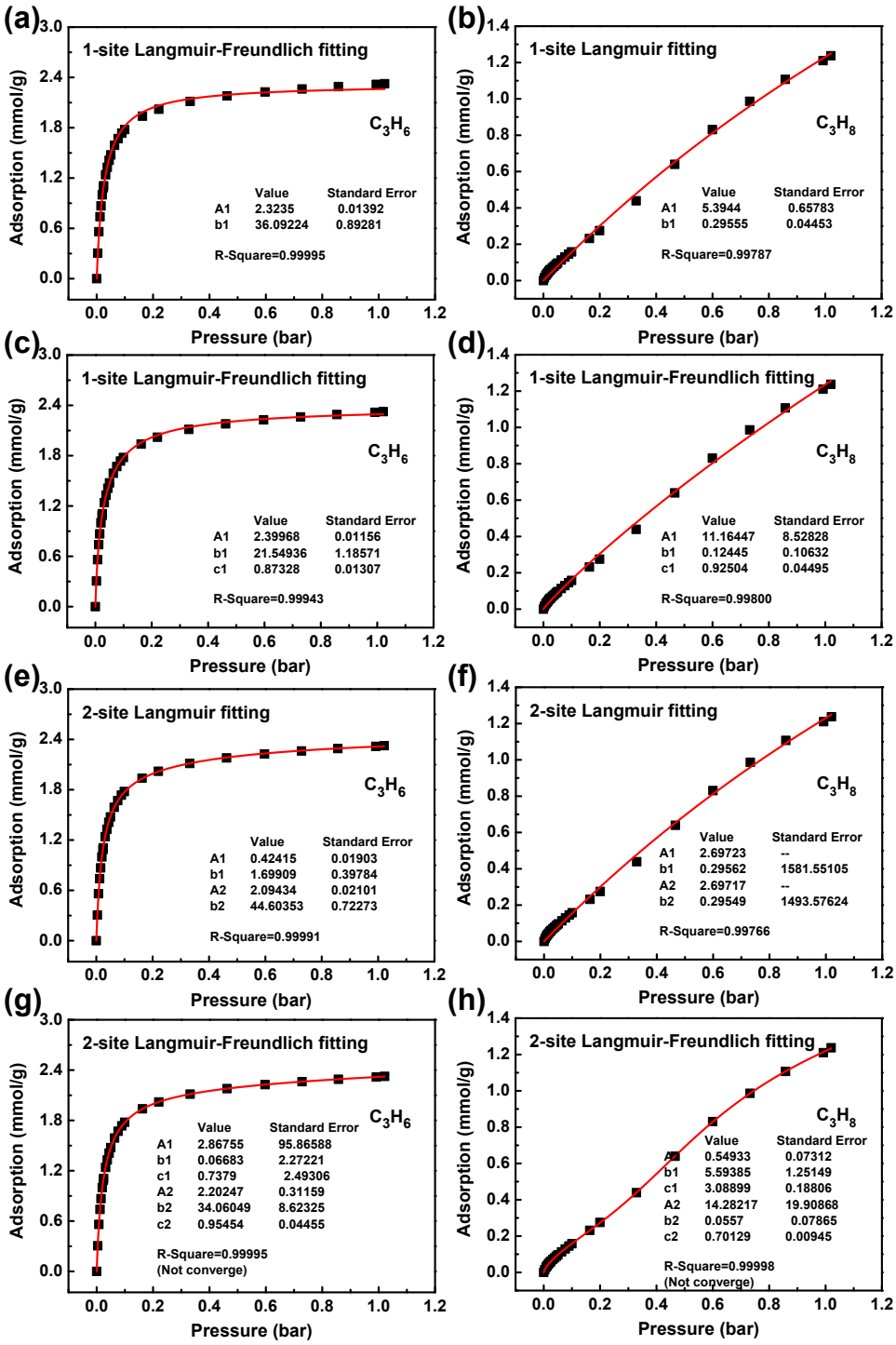

Figure S9. Fitting curves for C_3H_6 and C_3H_8 adsorption isotherms at 298 K and 1 bar based on different adsorption model, and fitting parameters of 1-site Langmuir-Freundlich model were used to calculate IAST selectivity for CoNi-piz.

5. IAST selectivity

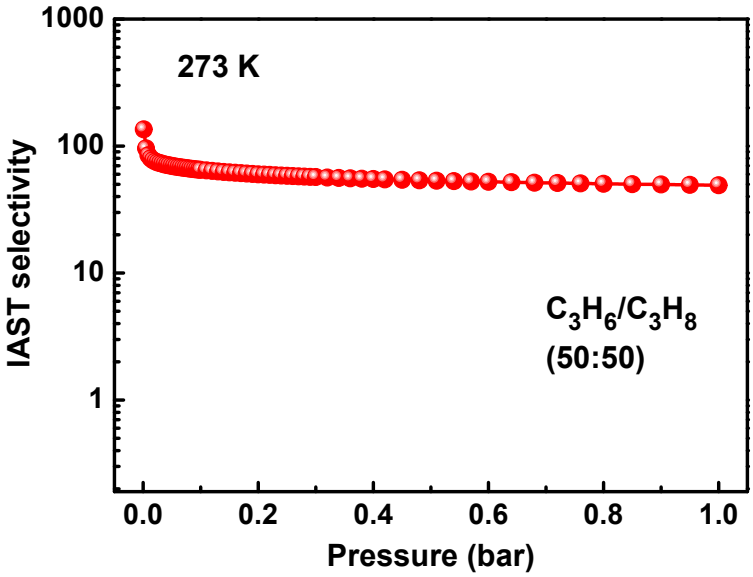

Figure S10. The calculated IAST selectivity for equimolar C_3H_6/C_3H_8 mixture at 273 K up to 1 bar.

6. Isosteric heat of adsorption

6.1. Virial fitting curves and the calculated adsorption heat for CoNi-pyz

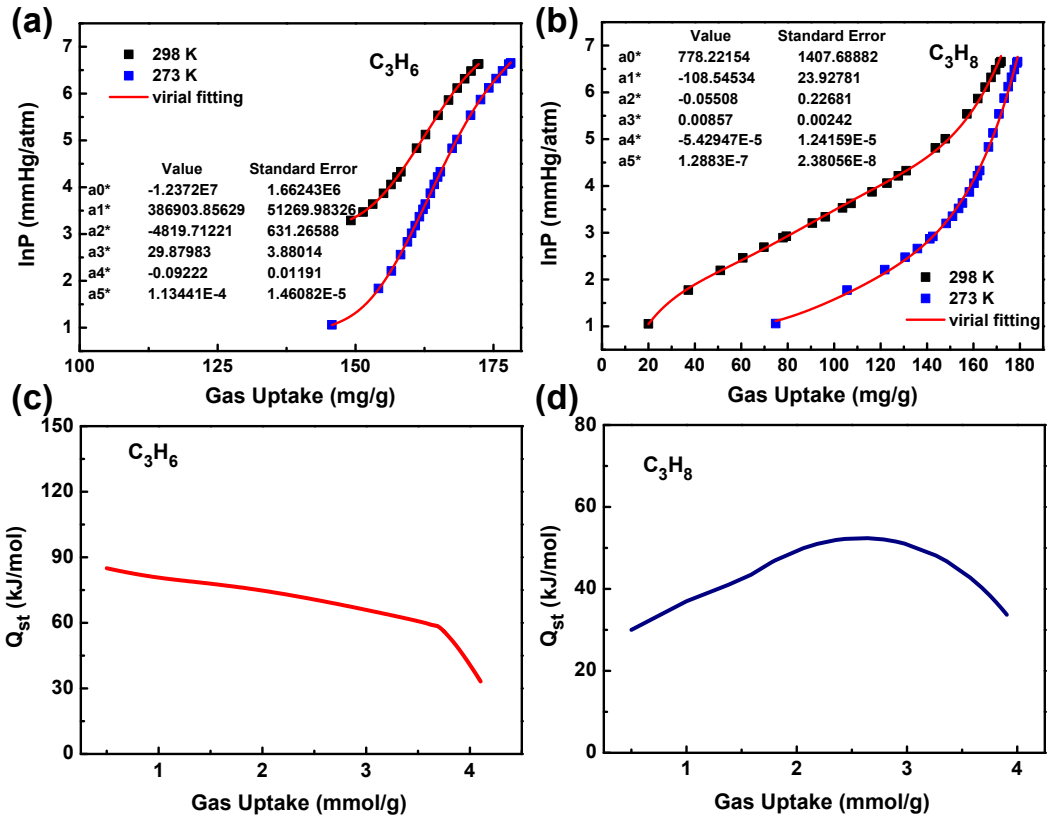

Figure S11. Virial fitting curves for adsorption isotherms of C_3H_6 (a) and C_3H_8 (b) at 298 K and 273 K up to 1 bar, and the adsorption heat for C_3H_6 (c) on CoNi-pyz is much higher than that of C_3H_8 (d) at zero coverage region.

6.2. Virial fitting curves and the calculated adsorption heat for CoNi-piz

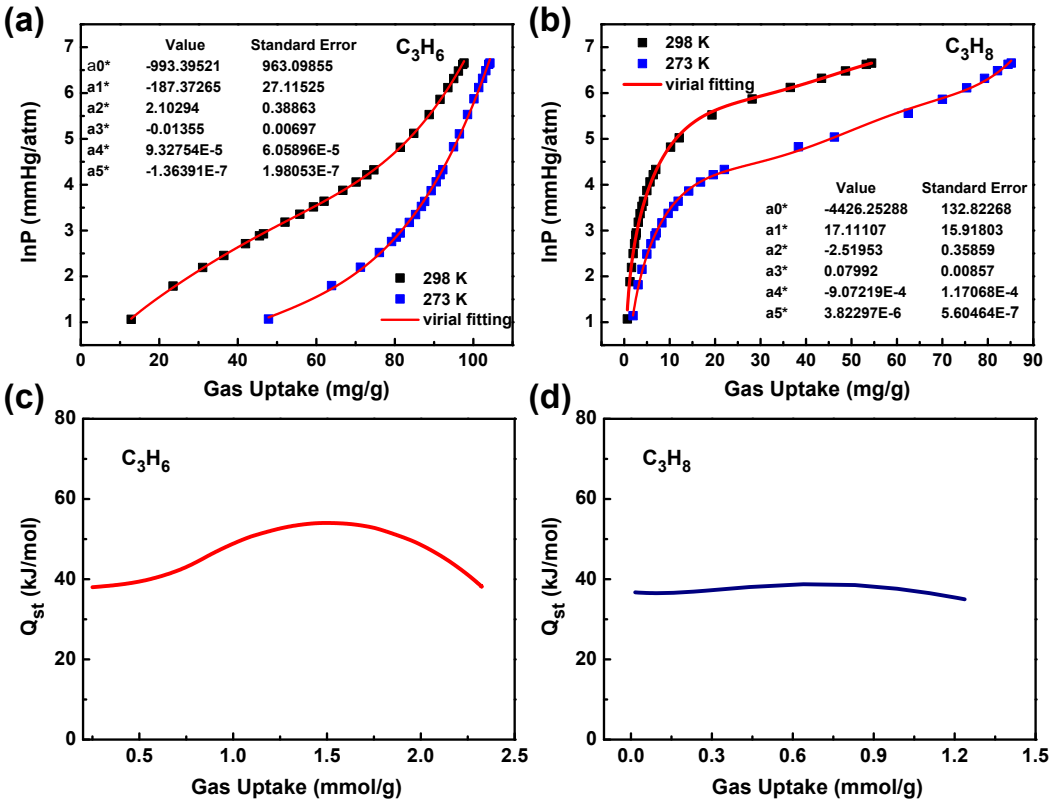

Figure S12. Virial fitting curves for adsorption isotherms of C_3H_6 (a) and C_3H_8 (b) at 298 K and 273 K up to 100 kPa, and the adsorption heat for C_3H_6 (c) on CoNi-piz is much lowered compared with that of CoNi-pyz.

7. Dynamic breakthrough experiment

Dynamic breakthrough experiments were carried out on a homemade instrument, as illustrated in Figure S13. The activated shaped MOF (40-60 mesh) particle was loaded into the adsorption column, which was maintained at 298 K by a thermostat. Then the Helium was used to pump out other gas inside to purify the adsorbents. After leak detection, the mixed gas of equimolar C_3H_6 and C_3H_8 (50/50, v/v) flowed over the adsorption column at a rate of 2 mL/min and the effluent gas stream from the outlet was monitored by gas chromatography (GC-2014C) constantly with a thermal conductivity detector (TCD). For the cycling breakthrough experiment, the adsorption column was regenerated by purging in situ with Helium at a flow rate of 30 mL/min for 2 h at 298 K, then the breakthrough experiment was conducted. (adsorbent mass: 0.6637 g and 0.4571 g for CoNi-piz and CoNi-pyz; and the corresponding adsorption column specifications are φ4×70 mm and φ4×59 mm respectively).

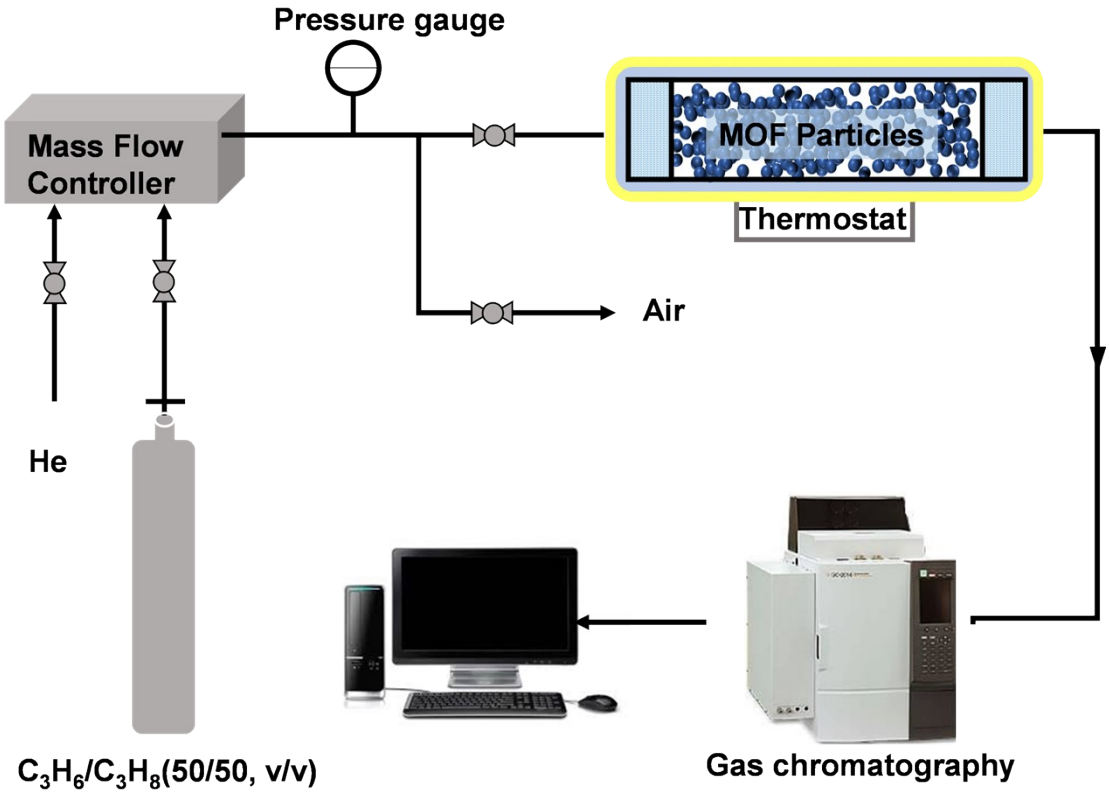

Figure S13. The breakthrough experimental apparatus.

8. Dynamic adsorption and desorption for C_3H_6 and C_3H_8

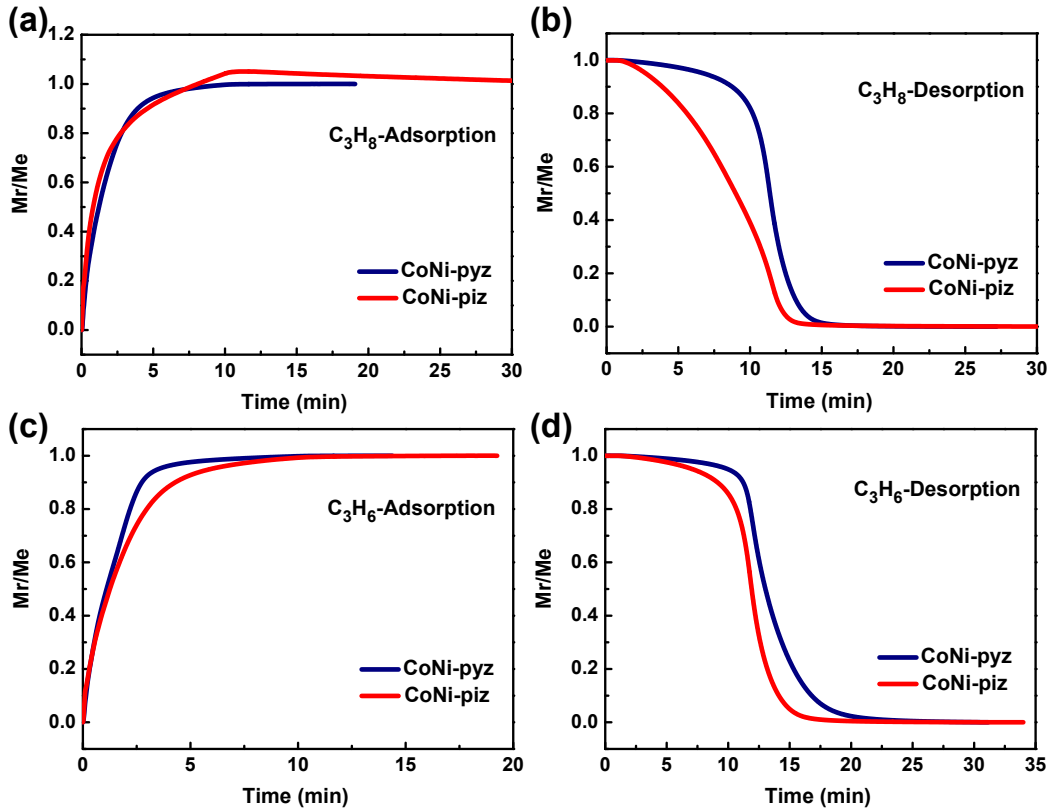

Figure S14. Dynamic adsorption for C_3H_6 and C_3H_8 at 298 K and 100 kPa on CoNi-pyz and CoNi-piz respectively. The slope of the isotherm indicates the adsorption rate for two components, which demonstrates the faster adsorption rate of C_3H_6 compared to C_3H_8.

9. Dynamic breakthrough experiment under water vapor.

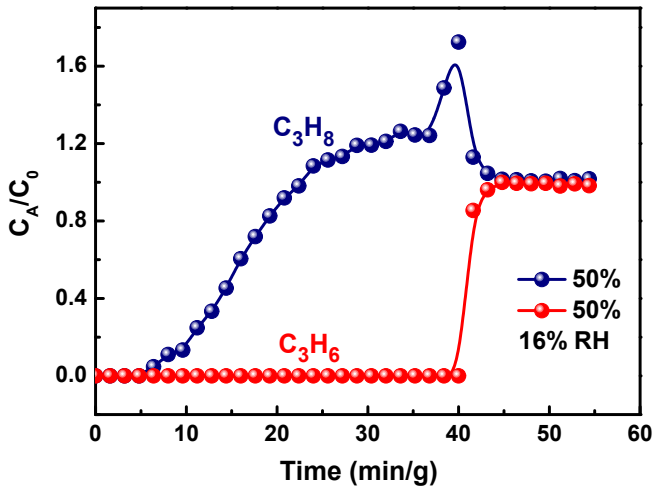

Figure S15. Dynamic breakthrough experiment for equimolar C_3H_6/C_3H_8 mixture under 16% relative humidity with a gas flow rate of 2 mL/min.

10. Supplementary tables

Table S1. Comparison for molecular sizes and physical properties of C_3H_6 and C_3H_8

Compounds	Ball and Stick model	Dimensions (Å^3)	Kinetic Diameter (Å)	Boiling point (K)
C_3H_8	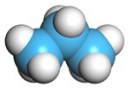	6.80×4.20×4.60	5.1	231.1
C_3H_6	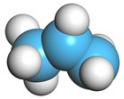	6.44×4.65×4.16	4.7	225.5

Table S2. Fitting parameters of single-site Langmuir-Freundlich isotherm model for C_3H_6 and C_3H_8 adsorption on CoNi-pyz at 298 K and 100 kPa.

	$q_{sat,A}$	b_A	v_A	R-Square
	mmol·g^{-1}	bar^{-1}	dimensionless	
C_3H_6	4.03054	350.0529	1.23859	0.99083
C_3H_8	4.01759	24.1528	0.91886	0.99956

Table S3. Fitting parameters of single-site Langmuir-Freundlich isotherm model for C_3H_6 and C_3H_8 adsorption on CoNi-piz at 298 K and 100 kPa.

	$q_{sat,A}$	b_A	v_A	R-Square
	mmol·g^{-1}	bar^{-1}	dimensionless	
C_3H_6	2.39968	21.54936	0.87328	0.99943
C_3H_8	11.16447	0.12445	0.92504	0.99800

Table S4. Fitting parameters of single-site Langmuir-Freundlich isotherm model for C_3H_6 and C_3H_8 adsorption on CoNi-pyz at 273 K and 100 kPa.

	$q_{sat,A}$	b_A	v_A	R-Square
	mmol·g^{-1}	bar^{-1}	dimensionless	
C_3H_6	5.33157	3.74983	0.11534	0.99907
C_3H_8	4.03597	93.81032	0.85816	0.99771

Table S5. Fitting parameters of single-site Langmuir-Freundlich isotherm model for C_3H_6 and C_3H_8 adsorption on CoNi-piz at 273 K and 100 kPa.

	$q_{sat,A}$	b_A	v_A	R-Square
	mmol·g^{-1}	bar^{-1}	dimensionless	
C_3H_6	2.49974	38.57111	0.66881	0.99665
C_3H_8	2.23093	6.44072	1.28231	0.99764

10.1. Dynamic capture capacity for C_3H_6 and C_3H_8 at mixed gas condition.

To determine the adsorption amount at the mixed gas condition, the dynamic

saturated adsorption capacity of each component ($q_{i,m}$) is calculated based on the breakthrough curves by the equation described as follows:

$$q_{i,m} = \frac{\int_0^{t_0} (F_i - F_e)\Delta t - V_{dead}}{m} \quad (1)$$

Where the F_i is the flow rate of specific gas at the inlet of the adsorption column with the unit of mL/min, while the F_e represent the effluent flow rate of the corresponding gas species; V_{dead} is the dead volume of the system (cm^3); And m represents the mass of the adsorbent loaded into the adsorption column (g); t_0 is the retention time interval for the gas mixture.

Table S6. Dynamic adsorption amount for C_3H_6 and C_3H_8 on CoNi-pyz and CoNi-piz respectively based on the breakthrough experiment for equimolar C_3H_6/C_3H_8 mixture.

	C_3H_6/C_3H_8 mixture	
	CoNi-pyz	CoNi-piz
C_3H_6 (cm^3/g)	77.7	35.6
C_3H_8 (cm^3/g)	58.0	19.0

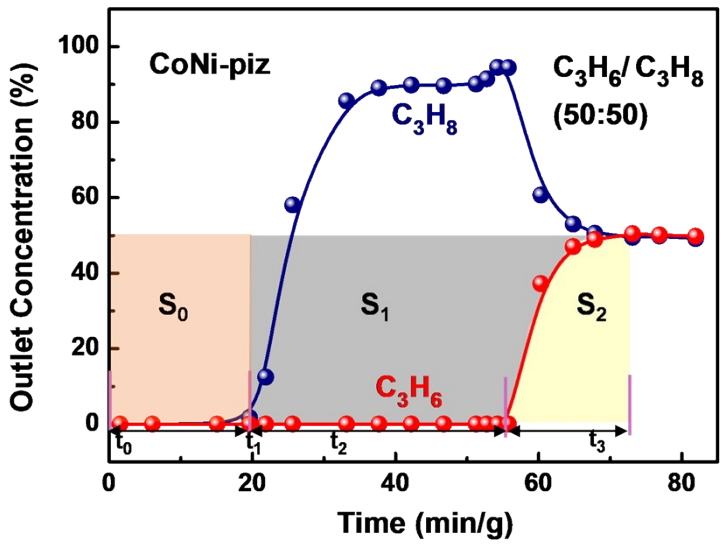

Figure S16. Dynamic adsorption calculation for C_3H_6 and C_3H_8 at 298 K and 100 kPa

based on the breakthrough experiment for CoNi-piz.

According to the equation above, here we take the C_3H_6/C_3H_8 (50/50, v/v) mixture as an example to show the calculation detail. The C_3H_8 adsorption amount was demonstrated as the orange area (S_0), thus $q_{C3H8}=F_e\ (t_1-t_0)\times 0.5=19\ cm^3/g$; While for C_3H_6 adsorption, we integrated the area of (S_0+S_1), and its capture amount was 35.6 cm^3/g.

Table S7. Comparison among adsorbents for C_3H_6/C_3H_8 separation at 298 K and 100 kPa.

Adsorbents	C_3H_6 adsorption	C_3H_8 adsorption	$Q_{st,C3H6}$	$Q_{st,C3H8}$	Selectivity (50/50)	Ref.
	mmol·g^{-1}	mmol·g^{-1}	kJ·mol^{-1}	kJ·mol^{-1}		
$Cu_3(BTC)_2$	7.7 (323 K)	6.6 (323 K)	42	28	23.1[b] (323 K)	S1
MIL-100(Fe)	1.4 (303 K)	0.6 (303 K)	70[c]	30[c]	28.9 (313 K)	S2
MIL-101(Cr)	3.94 (313 K)	2.2 (313 K)	\	\	6.0 (313 K)	S3
Mg-MOF-74	8.2	7.1	60.5	33.9	18.7[b]	S4
Co-MOF-74	5.9 (296 K)	5.2 (296 K)	53.0	47.0	8.6 (296 K)	S5
Mn-MOF-74	6.0	4.5	48.0	34.0	24	S6
Fe-MOF-74	6.8 (318 K)	6.0 (318 K)	44.0	33.0	13 (318 K)	S7
Ni-MOF-74	7.0 (318 K)	5.7 (318 K)	46	34	11.0 (318 K)	S8
Mn_2(m-dobdc)	7.1	5.8	67	38.0	39	S9
Fe_2(m-dobdc)	7.2	5.8	73	46	56	
Co_2(m-dobdc)	7.5	5.9	52	52	39	
Ni_2(m-dobdc)	7.2	6.0	54	45	35	
$[Zn_2(5\text{-aip})_2(bpy)]$	1.9	0.75	46.2	25.5	19.8	S10
ZIF-7	2.0	1.5	\	\	\	S11
ZIF-8	3.2 (0.5 bar, 303 K)	3.3 (0.5 bar, 303 K)	30	34	125[a]	S12
ZIF-67	4.6 (308 K)	4.8 (308 K)	25	26.4	200[a]	S13
NJU-Bai8	2.8	2.8	\	\	4	S14

ELM-12	1.47	1.36	30	28	204[a]	S15
DBTO	1.5	1.1	\	\	11[a]	S16
BTO	0.75	0.6	\	\	12[a]	
$Zn(ox)_{0.5}(trz)$	2.3 (303 K)	\	43	\	860 (303 K)[a]	S17
$Zn(ox)_{0.5}(atrz)$	1.7 (303 K)	\	\	\	175 (303 K)[a]	
$Co(IPA)(BPY)_{0.5}$	1.99	0.49	41.8	\	21	S18
Y-abtc	2.0	\	50	\	\	S19
HAIM-301	3.16	\	40	\	\	S20
KAUST-7	1.4	\	57.4	\	\	S21
JNU-3a	2.6	2.1	29.3[c]	16.1[c]	513	S22
Co-gallate	1.78	\	41	\	\	S23
CoNi-pyz	4.10	3.90	83	30	3	**This work**
CoNi-piz	2.32	1.23	38	36	15	

[a] Kinetic selectivity; [b] Calculated by the Herry constants for C_3H_6 and C_3H_8; [c] Measured by calorimetry

References

1. N. Lamia, M. Jorge, M. A. Granato, F. A. Almeida Paz, H. Chevreau and A. E. Rodrigues, Adsorption of propane, propylene and isobutane on a metal–organic framework: Molecular simulation and experiment, *Chem. Eng. Sci.*, 2009, **64**, 3246-3259.
2. J. W. Yoon, Y.-K. Seo, Y. K. Hwang, J.-S. Chang, H. Leclerc, S. Wuttke, P. Bazin, A. Vimont, M. Daturi, E. Bloch, P. L. Llewellyn, C. Serre, P. Horcajada, J.-M. Grenèche, A. E. Rodrigues and G. Férey, Controlled Reducibility of a Metal–Organic Framework with Coordinatively Unsaturated Sites for Preferential Gas Sorption, *Angew. Chem. Int. Ed.*, 2010, **49**, 5949-5952.
3. S.-J. Lee, J. W. Yoon, Y.-K. Seo, M.-B. Kim, S.-K. Lee, U. H. Lee, Y. K. Hwang, Y.-S. Bae and J.-S. Chang, Effect of purification conditions on gas storage and separations in a chromium-based metal–organic framework MIL-101, *Microporous Mesoporous Mater.*, 2014, **193**, 160-165.
4. Z. Bao, S. Alnemrat, L. Yu, I. Vasiliev, Q. Ren, X. Lu and S. Deng, Adsorption of Ethane, Ethylene, Propane, and Propylene on a Magnesium-Based Metal–Organic Framework, *Langmuir*, 2011, **27**, 13554-13562.
5. Y. He, R. Krishna and B. Chen, Metal–organic frameworks with potential for energy-efficient adsorptive separation of light hydrocarbons, *Energy Environ. Sci.*, 2012, **5**, 9107-9120.
6. Y.-S. Bae, C. Y. Lee, K. C. Kim, O. K. Farha, P. Nickias, J. T. Hupp, S. T. Nguyen and R. Q. Snurr, High Propene/Propane Selectivity in Isostructural Metal–Organic Frameworks with High Densities of Open Metal Sites, *Angew. Chem. Int. Ed.*, 2012, **51**, 1857-1860.
7. D. Bloch Eric, L. Queen Wendy, R. Krishna, M. Zadrozny Joseph, M. Brown Craig and R. Long Jeffrey, Hydrocarbon Separations in a Metal-Organic Framework with Open Iron(II) Coordination Sites, *Science*, 2012, **335**, 1606-1610.
8. S. J. Geier, J. A. Mason, E. D. Bloch, W. L. Queen, M. R. Hudson, C. M. Brown and J. R. Long, Selective adsorption of ethylene over ethane and propylene over propane in the metal–organic frameworks M2(dobdc) (M = Mg, Mn, Fe, Co, Ni, Zn), *Chem. Sci.*, 2013, **4**, 2054-2061.
9. J. E. Bachman, M. T. Kapelewski, D. A. Reed, M. I. Gonzalez and J. R. Long, M2(m-dobdc) (M = Mn, Fe, Co, Ni) Metal–Organic Frameworks as Highly Selective, High-Capacity Adsorbents for Olefin/Paraffin Separations, *J. Am. Chem. Soc.*, 2017, **139**, 15363-15370.
10. Y. Chen, H. Wu, D. Lv, N. Yuan, Q. Xia and Z. Li, A pillar-layer metal-organic framework for efficient adsorption separation of propylene over propane, *Sep. Purif. Technol.*, 2018, **204**, 75-80.
11. C. Gücüyener, J. van den Bergh, J. Gascon and F. Kapteijn, Ethane/Ethene Separation Turned on Its Head: Selective Ethane Adsorption on the Metal−Organic Framework ZIF-7 through a Gate-Opening Mechanism, *J. Am. Chem. Soc.*, 2010, **132**, 17704-17706.
12. K. Li, D. H. Olson, J. Seidel, T. J. Emge, H. Gong, H. Zeng and J. Li, Zeolitic Imidazolate Frameworks for Kinetic Separation of Propane and Propene, *J. Am. Chem. Soc.*, 2009, **131**, 10368-10369.
13. P. Krokidas, M. Castier, S. Moncho, D. N. Sredojevic, E. N. Brothers, H. T. Kwon, H.-K. Jeong, J. S. Lee and I. G. Economou, ZIF-67 Framework: A Promising New Candidate for Propylene/Propane Separation. Experimental Data and Molecular Simulations, *J. Phys. Chem. C*, 2016, **120**, 8116-8124.
14. X. Wang, R. Krishna, L. Li, B. Wang, T. He, Y.-Z. Zhang, J.-R. Li and J. Li, Guest-dependent pressure induced gate-opening effect enables effective separation of propene and propane in a flexible MOF, *Chem. Eng. J.*, 2018, **346**, 489-496.

15. L. Li, R.-B. Lin, X. Wang, W. Zhou, L. Jia, J. Li and B. Chen, Kinetic separation of propylene over propane in a microporous metal-organic framework, *Chem. Eng. J.*, 2018, **354**, 977-982.
16. C. Y. Lee, Y.-S. Bae, N. C. Jeong, O. K. Farha, A. A. Sarjeant, C. L. Stern, P. Nickias, R. Q. Snurr, J. T. Hupp and S. T. Nguyen, Kinetic Separation of Propene and Propane in Metal−Organic Frameworks: Controlling Diffusion Rates in Plate-Shaped Crystals via Tuning of Pore Apertures and Crystallite Aspect Ratios, *J. Am. Chem. Soc.*, 2011, **133**, 5228-5231.
17. J. Peng, H. Wang, D. H. Olson, Z. Li and J. Li, Efficient kinetic separation of propene and propane using two microporous metal organic frameworks, *Chem. Commun.*, 2017, **53**, 9332-9335.
18. Y. Chen, H. Wu, L. Yu, S. Tu, Y. Wu, Z. Li and Q. Xia, Separation of propylene and propane with pillar-layer metal–organic frameworks by exploiting thermodynamic-kinetic synergetic effect, *Chem. Eng. J.*, 2021, DOI: https://doi.org/10.1016/j.cej.2021.133284, 133284.
19. H. Wang, X. Dong, V. Colombo, Q. Wang, Y. Liu, W. Liu, X.-L. Wang, X.-Y. Huang, D. M. Proserpio, A. Sironi, Y. Han and J. Li, Tailor-Made Microporous Metal–Organic Frameworks for the Full Separation of Propane from Propylene Through Selective Size Exclusion, *Adv. Mater.*, 2018, **30**, 1805088.
20. L. Yu, X. Han, H. Wang, S. Ullah, Q. Xia, W. Li, J. Li, I. da Silva, P. Manuel, S. Rudić, Y. Cheng, S. Yang, T. Thonhauser and J. Li, Pore Distortion in a Metal–Organic Framework for Regulated Separation of Propane and Propylene, *J. Am. Chem. Soc.*, 2021, **143**, 19300-19305.
21. A. Cadiau, K. Adil, P. M. Bhatt, Y. Belmabkhout and M. Eddaoudi, A metal-organic framework–based splitter for separating propylene from propane, *Science*, 2016, **353**, 137-140.
22. H. Zeng, M. Xie, T. Wang, R.-J. Wei, X.-J. Xie, Y. Zhao, W. Lu and D. Li, Orthogonal-array dynamic molecular sieving of propylene/propane mixtures, *Nature.*, 2021, **595**, 542-548.
23. B. Liang, X. Zhang, Y. Xie, R.-B. Lin, R. Krishna, H. Cui, Z. Li, Y. Shi, H. Wu, W. Zhou and B. Chen, An Ultramicroporous Metal–Organic Framework for High Sieving Separation of Propylene from Propane, *J. Am. Chem. Soc.*, 2020, **142**, 17795-17801.